FDTD Modeling of Common-Mode Radiation from Cables

David M. Hockanson, *Student Member, IEEE,* James L. Drewniak, *Member, IEEE,* Todd H. Hubing, *Senior Member, IEEE,* and Thomas P. Van Doren, *Member, IEEE*

***Abstract*— Radiation from cables attached to printed circuit boards and shielding enclosures is among the primary concerns in meeting FCC Class A and B limits. The finite-difference time-domain (FDTD) method can be employed to model radiation from printed circuit boards and shielding enclosures with complex geometries, but difficulties in modeling wires and cables of arbitrary radii are encountered. Modeling the wire by setting the axial component of the electric field to zero in the FDTD method results in an effective wire radius that is determined by the mesh discretization. Neglecting the wire radius in applications, such as electromagnetic interference (EMI) or printed circuit board modeling, may result in gross errors because near-field quantities are typically sensitive to wire thickness. Taflove *et al.* have developed a subcellular FDTD algorithm for modeling wires that has been shown to work well for plane wave scattering. The method uses a quasistatic field approximation to model wires with a well defined radius independent of the mesh dimensions. The wire model is reviewed and investigated for application to common-mode radiation from cables attached to printed circuit boards, where the source is often a noise voltage at the connector. Also investigated is energy coupling to attached cables through enclosure apertures resulting in common-mode radiation from the cable. The input impedance for a center-fed dipole antenna, as well as a monopole connected to a conducting half-sheet, is computed with FDTD methods and compared to moment method input impedance results. A simulation of a shielding enclosure with an attached cable demonstrates the utility of FDTD analysis in modeling common-mode radiation.**

I. Introduction

THE finite-difference time-domain (FDTD) method has been successfully applied to many electromagnetic scattering problems including radar cross section (RCS), antennas, microwave circuits, and EMC, among others. The reader is referred to [1] and [2] for information on FDTD.

Common-mode radiation from cables attached to printed circuit boards and shielding enclosures is a primary source of electromagnetic interference, although direct radiation from slots and apertures is also of concern, and will become more problematic as clock frequencies and edge rates increase. Typical high-speed printed circuit designs with attached cables are too complex to model in great detail with present generation computers. Further, mechanisms that couple signals from IC sources to common-mode currents on cables are not well understood [3]. However, one mechanism of common-mode radiation can be modeled with a noise voltage source at the connector, which drives an attached cable against the printed circuit board ground plane, or the shielding enclosure [4], [5]. By adequately modeling the EMI "antenna," resonance frequencies can be predicted, as well as the effectiveness of series loading the cable with a ferrite sleeve. In addition, with a sufficient model for the noise voltage source, EMI can be predicted with engineering accuracy.

Conducting enclosures are designed to minimize radiated emissions from digital electronics. However, the shielding integrity of the enclosures is compromised by cooling vents, connectors, seams, and display apertures, among other perforations. In addition to radiation directly through the apertures, energy may be coupled through an aperture to an attached shielded or unshielded cable. Radiated emissions can be increased as a result of the cable increasing the Q of a resonance, as well as the cable serving to direct energy. Common-mode radiation from cables attached to printed circuit boards or enclosures will be greatest at and near a resonance of the EMI antenna, one portion of which is the attached cable. Inadequately modeling the cable length or radius can result in a significant shift in predicted resonance frequencies. Such a shift can move the predicted resonance away from a harmonic of a clock that may be driving the common-mode current on the attached cable, resulting in a failure to predict a potential EMI problem. Conversely, a shift in the calculated resonance frequency can result in predicting a problem where one may not exist. A subcellular FDTD model for wires is needed to numerically study coupling mechanisms present in complicated electromagnetic structures with external cables without discretizing down to the wire diameter.

Previous work on modeling wires with the FDTD method has been reported. Accurate results have been achieved by modeling with a very fine discretization in the region of the wire and setting the axial component of the electric field to zero [6]. However, this approach does not permit modeling of wires with specific diameters; rather, the diameter is determined by the mesh discretization. Further, considerable computational resources are expended in discretizing down to the wire diameter. Another method involves calculating the self-inductance of a segment of wire and developing FDTD equations for computing the necessary field quantities [7]. This approach is not computationally efficient for large problems because additional charge and current equations are introduced. A quasistatic subcellular algorithm for modeling wires has been successfully employed in FDTD for modeling plane-wave scattering from wires [8], [9]. Luebbers *et al.* used this approach to model a monopole on a conducting box [10];

Manuscript received June 23, 1995; revised April 2, 1996.

The authors are with the Department of Electrical Engineering, Electromagnetic Compatibility Laboratory, University of Missouri-Rolla, Rolla, MO 65401 USA.

Publisher Item Identifier S 0018-9375(96)06138-8.

0018–9375/96$05.00 © 1996 IEEE

however, they encountered difficulties in modeling the source region.

Taflove's subcellular algorithm for modeling wires and cable bundles is reviewed and investigated here for use in modeling common-mode radiation from cables attached to printed circuit boards and enclosures where the noise voltage source is at the connector. A dipole antenna is modeled with the FDTD method, and the input impedance is calculated and compared with results from the numerical electromagnetics code (NEC) [11]. These results show that a common practice of modeling wires by setting tangential electric field components to zero along a line of FDTD cells results in wire dimensions determined by the mesh discretization. A model for the source region is also presented and investigated with dipole input impedance results. A monopole attached to a conducting half-sheet, which is more indicative of antenna geometries at the printed circuit board level, is also modeled, and the FDTD input impedance results are compared with published moment method results [12]. The quasistatic algorithm is found to predict the input impedance with reasonable accuracy for wires less than three-quarters of a wavelength long, and near odd-integer half-wavelength lengths. Since input impedance is a sensitive function of the near-fields, the quasistatic subcellular algorithm for modeling wires or cables is expected to yield a good approximation for computed field strengths at FCC distances.

Moment methods have been effectively applied to cavities with apertures for RCS analysis [13], [14]. Common-mode radiation from an enclosure with an aperture and attached cable is modeled herein using FDTD. The power radiated through the aperture is computed with and without the attached cable. The results show that an attached cable can "tune" system resonances resulting in increased radiation.

II. Review of the Taflove *et al.* FDTD Subcellular Thin Wire Model

Proper consideration must be given to wire modeling to enable accurate computation of near-field parameters. Wires are placed along the electric field grid of the FDTD mesh because the tangential component of the electric field on the surface of a perfect electric conductor (pec) is zero. Modeling the wire by setting the axial component of the electric field to zero is found from numerical simulations to yield effective wire radii of approximately 20% of a cell length for cubic cells (see Section III). An effective radius results because the FDTD algorithm averages field values over a finite volume. An alternative to setting $\vec{E}_{\tan} = 0$ along an $\vec{E}$-field grid line, and having the wire radius determined by the mesh dimensions, is to employ a quasistatic approximation introduced for FDTD by Taflove *et al.* [9]. This approach is summarized briefly herein.

A wire superimposed on a Yee mesh, and discrete field locations in the plane of the wire are shown in Fig. 1. For small cells, the electric field component parallel to the wire $E_z(i+1)$, can be approximated as a linear function in z. A quasistatic approximation $(1/r)$ is employed for the functional variation of the fields in the direction radial to the wire axis. The fields over a unit cell can then be expressed approximately

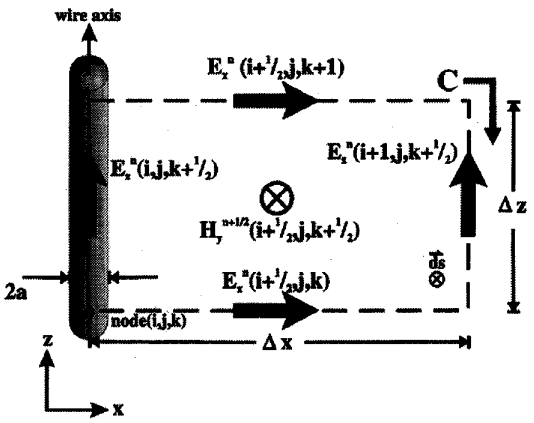

Fig. 1. Discrete Yee-mesh field locations in the plane of a thin wire.

as [15]

$$E_z^n(i,j;z) = 0 \tag{1a}$$

$$E_z^n(i+1,j;z) = E_z^n\left(i+1,j,k+\frac{1}{2}\right) \times \left[1 - c\left(z - \frac{\Delta z}{2}\right)\right] \tag{1b}$$

$$E_x^n(x;j,k) = E_x^n\left(i+\frac{1}{2},j,k\right)\frac{\frac{\Delta x}{2}}{x} \tag{1c}$$

$$E_x^n(x;j,k+1) = E_x^n\left(i+\frac{1}{2},j,k+1\right)\frac{\frac{\Delta x}{2}}{x} \tag{1d}$$

$$H_y^{n+(1/2)}(x;j;z) = H_y^{n+(1/2)}\left(i+\frac{1}{2},j,k+\frac{1}{2}\right)\frac{\frac{\Delta x}{2}}{x} \times \left[1 - c\left(z - \frac{\Delta z}{2}\right)\right] \tag{1e}$$

where c is an arbitrary constant that is eliminated in the derivation of the time-marching scheme. Substituting the above expressions into the integral form of Faraday's law

$$\oint_C \vec{E}\cdot\vec{dl} = -\frac{\partial}{\partial t}\iint_S \mu\vec{H}\cdot\vec{ds} \tag{2}$$

yields

$$\begin{aligned}
&\int_a^{\Delta x} E_x^n\left(i+\frac{1}{2},j,k+1\right)\frac{\frac{\Delta x}{2}}{x}\,dx \\
&\quad + \int_{\Delta z}^{0} E_z^n\left(i+1,j,k+\frac{1}{2}\right)\left[1 - c\left(z-\frac{\Delta z}{2}\right)\right]dz \\
&\quad + \int_{\Delta x}^{a} E_x^n\left(i+\frac{1}{2},j,k\right)\frac{\frac{\Delta x}{2}}{x}\,dx \\
&= -\frac{\partial}{\partial t}H_y^n\left(i+\frac{1}{2},j,k+\frac{1}{2}\right) \\
&\quad \times \int_0^{\Delta z}\int_a^{\Delta x} \mu\frac{\frac{\Delta x}{2}}{x}\left[1 - c\left(z-\frac{\Delta z}{2}\right)\right]dx\,dz
\end{aligned} \tag{3}$$

where the integration paths are shown in Fig. 1. Evaluating (3) and rearranging yields a time-marching equation for H_y near a thin wire of radius a oriented in the $\hat{z}$ direction as

$$H_y^{n+(1/2)}\left(i+\frac{1}{2},j,k+\frac{1}{2}\right) = H_y^{n-(1/2)}\left(i+\frac{1}{2},j,k+\frac{1}{2}\right) - \frac{\Delta t}{\mu}\left[\frac{E_x^n(i+\frac{1}{2},j,k+1)-E_x^n(i+\frac{1}{2},j,k)}{\Delta z} - \frac{E_z^n(i+1,j,k+\frac{1}{2})}{\frac{\Delta x}{2}\ln\frac{\Delta x}{a}}\right]. \quad (4a)$$

The other three magnetic field components surrounding the wire are obtained similarly. Similar equations can be developed for the magnetic fields circulating thin wires with orientations in the $\hat{x}$ and $\hat{y}$ directions. This subcellular algorithm for modeling wires is attractive, because of its computational efficiency and simplicity.

III. Thin Wire Model Evaluation

The subcellular wire modeling algorithm developed by Taflove *et al.* was investigated for near-field computations useful for EMI and EMC analysis. The accuracy of the thin-wire algorithm for predicting input impedance was evaluated by modeling two different configurations. First, a dipole antenna was investigated, and the input impedance was calculated for a center-fed dipole over a range of frequencies. The antenna was modeled using FDTD and the subcellular wire algorithm, and compared to results obtained with the NEC [11]. Second, a wire extending from a semi-infinite ground plane was investigated with FDTD . The FDTD results were compared to the moment method results of Sawaya *et al.* [12] for several different wire radii.

A. Center-Fed Dipole Antenna

Fig. 2 shows the dipole antenna that was numerically modeled with NEC and the FDTD method. The FDTD model of the source differed from that of the moment method code in that the FDTD source had a finite length (the length of a cell side), while the moment method employs a delta-gap generator source [16]. However, the mesh dimensions were kept small for the FDTD simulations to minimize discrepencies resulting from this modeling difference. The input impedance of the antenna was calculated as a function of the ratio of length L, to wavelength λ, over the range $0.25 \leq L/\lambda \leq 2$. Other dimensions are given in terms of the ideal half-wave resonance wavelength, which is denoted by $\lambda_o \equiv 2L$.

The antenna was first modeled by setting the axial electric field component on the wire axis to zero, and computing the surrounding magnetic field components with the usual free-space FDTD equations. Cubic cells were used with a

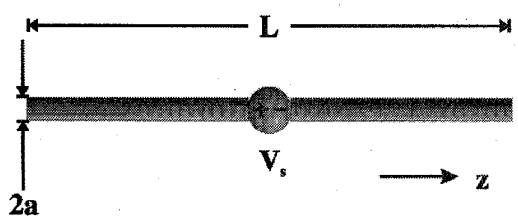

Fig. 2. Geometry of the dipole antenna model.

spatial discretization of $\Delta l = \lambda_o/42$, and a differential time element of $\Delta t \approx \Delta l/2c_o$,[1] where c_o is the free-space phase velocity. A sinusoidal steady-state source was employed. The antenna length remained fixed at each simulation frequency, and was 21 Yee cells long. Second-order Mur absorbing boundary conditions were placed a half-wavelength from the antenna. Perfectly Matched Layers (PML's) were also used as absorbing boundaries [17], and although no differences were observed in the results, the run-time to achieve steady-state was reduced by 75%. The simulations ran more quickly with the PML's because the PML's were constructed eight cells from the antenna, thereby reducing the size of the computational domain. The input impedance for the FDTD model was calculated using discrete Fourier transform techniques after the system reached steady-state for each frequency of interest.

The input impedance for a center-fed dipole antenna computed with the usual Yee FDTD algorithm is compared with NEC results in Fig. 3. With the electric field along the wire axis set to zero, seemingly approximating an infinitely thin wire, the FDTD method effectively models a wire of finite thickness. This results because the FDTD method computes the *average* of the field component over the volume of a cell and assigns it to a location associated with the unit cell. The averaging process results in an effective wire radius. Fig. 3 shows that the FDTD results agree best with the NEC results for a wire of radius $a = 0.005\lambda_o$. The effective radius of a wire is then approximately twenty percent of the cell dimension. Changing the discretization resulted in an effective radius that was still approximately 20% of the cell. The half-wave resonance frequency computed with FDTD differed by less than three percent from that computed with NEC for an antenna with a radius $a = 0.005\lambda_o$ (approximately 20% of the FDTD cell dimension). The half-wave resonance is important because the first resonance of a system will typically have the lowest impedance, resulting in greater radiation. Accurate prediction of the low-impedance resonance frequencies is necessary if common-mode radiation problems are to be numerically studied.

The subcellular wire algorithm of Taflove *et al.* was also employed for modeling thin wires. The wire radius can then be well defined. Fig. 4 shows a comparison of input impedance results for a center-fed dipole from FDTD and NEC, when the FDTD model included conductors with a well-defined radius.

[1]The differential time element was minutely changed at each frequency to allow an integer number of time steps per temporal period. An integer number of time steps is necessary for accurately computing frequency-domain quantities with the discrete Fourier transform.

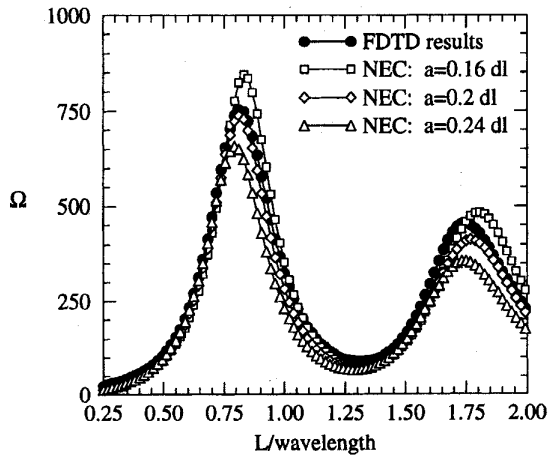

(a)

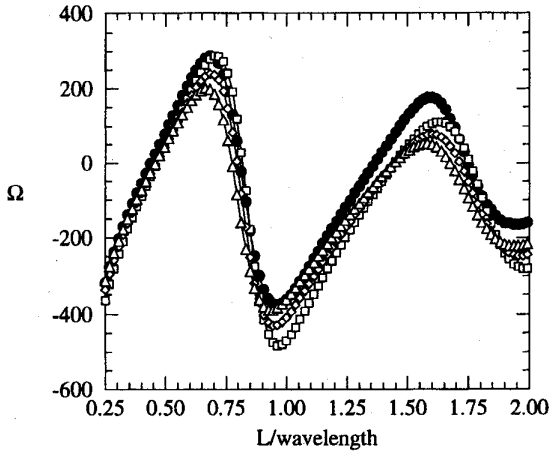

(b)

Fig. 3. FDTD input impedance comparisons for an antenna modeled without defining a radius for (a) input resistance, and (b) input reactance ($dl \equiv$ FDTD cell length).

The magnetic field components circulating the source (modeled with one Yee cell) were calculated with free-space FDTD time-marching equations. The magnetic field components surrounding the wire were computed with Taflove's quasistatic approximations. Although reasonably good agreement between the FDTD and NEC results was achieved for a moderately *thin* wire ($a = 0.2\Delta l$), the agreement was poor for *thick* ($a = 0.48\Delta l$) or *very thin* ($a = 0.02\Delta l$) wires. The *thick*[2] wire input resistances at resonance differed by approximately 100%. These discrepancies resulted from an inaccurate source model.

A more accurate source model was obtained by specifying the same radius for the source as the conductors using the quasistatic approximations of Taflove *et al.* The input impedance for a center-fed dipole was then computed for wires of three different radii. The FDTD results employing the improved source model are compared with the NEC results in Fig. 5.

[2]The names of the wires were chosen to denote the wire thicknesses relative to a cell size.

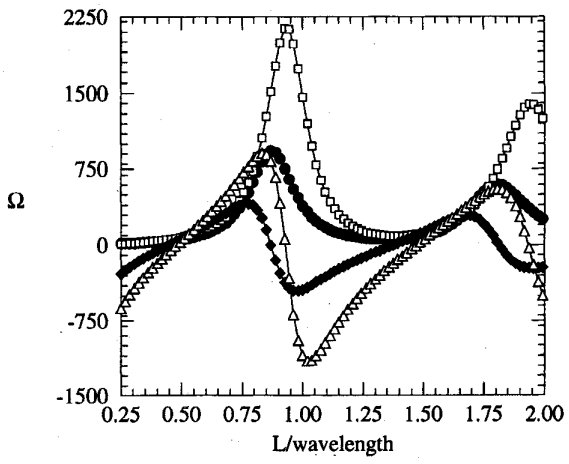

(a)

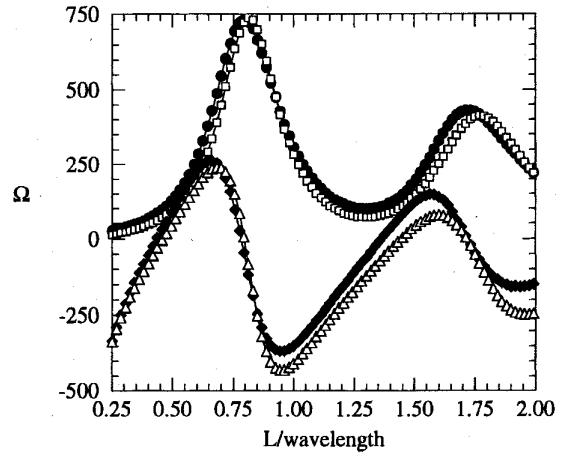

(b)

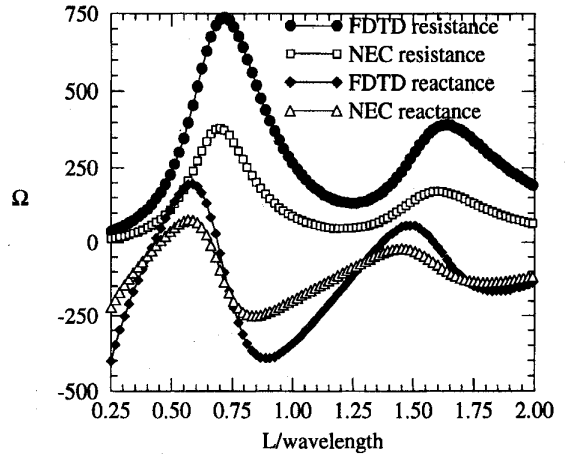

(c)

Fig. 4. Input impedance comparison between FDTD results and NEC results for a dipole antenna with a set conductor radius, but no well-defined source radius for (a) *very thin*, $a = 0.02\Delta l = \lambda_o/2,100$, (b) *thin*, $a = 0.2\Delta l = \lambda_o/210$, and (c) *thick*, $a = 0.48\Delta l = \lambda_o/87.5$ wires.

The *thin* wire ($a = 0.2\Delta l$) results still agreed well with the NEC results for dipole lengths less than approximately

$\frac{3}{4}\lambda$, as well as near odd-integer half-wavelength frequencies. The FDTD-computed half-wavelength resonance frequency was within three percent of that computed by NEC, and the input resistance at resonance was within one percent. A noticable improvement in the comparison between the FDTD results and NEC results for the *very thin* and *thick* wires was also obtained by defining the source radius. The *very thin* and *thin* wire results agreed well with the NEC computations up to approximately $L = \frac{3}{4}\lambda_o$, and the *thick* wire results agreed moderately well with NEC near odd-integer half-wavelength frequencies. The half-wavelength resonance frequency computed with FDTD was within five percent for both the *very thin* and *thick* wires, and the resistance at resonance was within three percent.

The results compared favorably in the vicinity of odd-integer half-wave resonances with discrepencies near full-wave resonances. The error is a consequence of the averaging property of FDTD field calculations. The field value computed with the FDTD algorithm is the average field value over the volume of a cell. The magnitude of the current is at a maximum at the source at odd-integer half-wave resonances, and has a moderate slope around the source. The FDTD method can adequately model the slow variation in the current around the source for odd-integer half-wave resonances because the average of a field component over the volume of a cell is very close to the field value at any point within the cell volume. By contrast, the current magnitude is a minimum at the source at full-wave resonance with a steep gradient in the vicinity of the source. The magnetic field components circling the source computed with the FDTD method are higher than the true value because of averaging, yielding a higher computed current value, which results in a lower impedance value. The current gradient for a thinner wire is steeper near the source than a thicker wire [18], resulting in greater errors in the FDTD calculations for the *very thin* wire model compared to the *thick* wire model. Therefore, the FDTD algorithm calculates odd-integer half-wave resonance frequencies and resistances with minimal error. The calculations near full-wave resonances are highly dependent on the details of the source model.

Noise sources at the printed circuit level that result in common-mode radiation are typically low-impedance sources [5]. Common-mode radiation from "dipole-type" antennas is then of most concern for lower EMI antenna input impedances that occur at odd-integer half-wavelength resonances. Consequently, it is not as great a concern that the full wave resonance can not be as accurately modeled since a noise voltage source will drive little common-mode current on the antenna as a result of the large input impedance.

The quasistatic approximation limits the wire radius to $a < \Delta l/2$, because calculation of magnetic field components circling the wire becomes unstable when the wire radius approaches the location of the magnetic field components encircling the wire. The field dependence does not have the same r variation if the fields are located inside the wire. The approximation might be reformulated for the case of wires with radii greater than $\Delta l/2$. Such a wire may be more easily modeled with a complete cell setting all tangential electric field components on the cell to zero, although this does not circumvent the problem of modeling a wire with a well-defined radius.

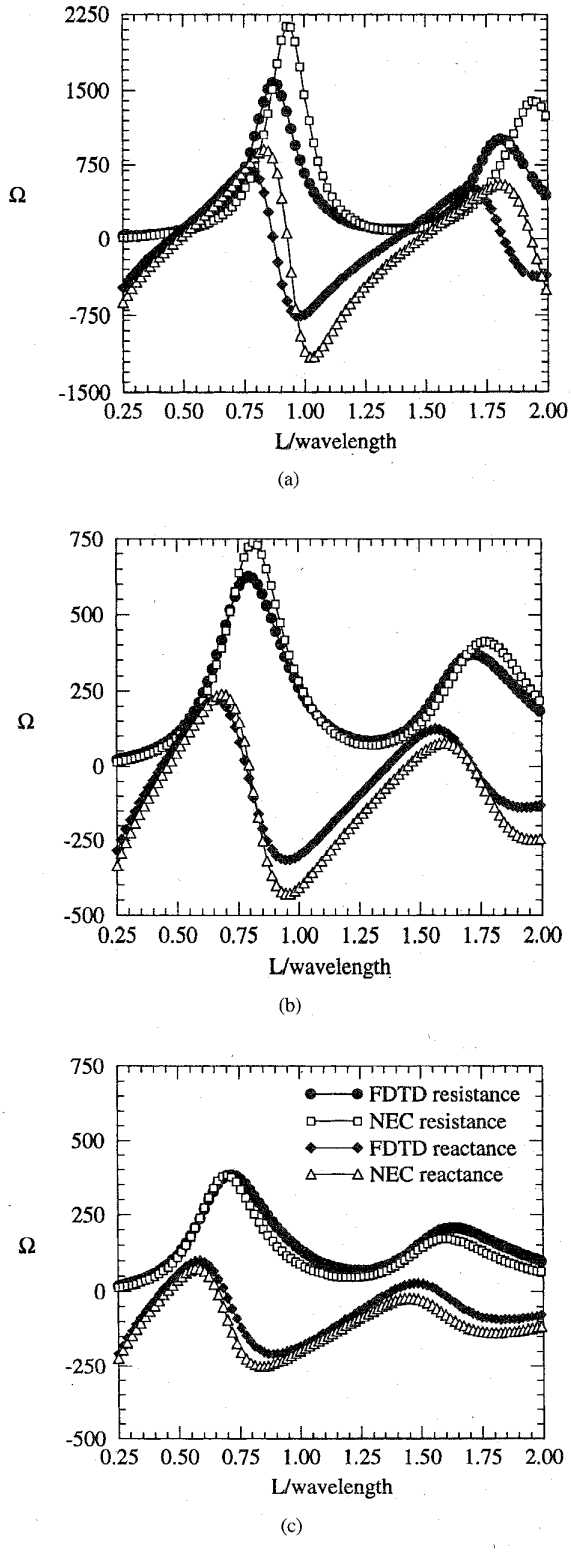

Fig. 5. Input impedance comparison between FDTD results and NEC results for a dipole antenna with set source and conductor radii for (a) *very thin*, $a = 0.02\Delta l = \lambda_o/2,100$, (b) *thin*, $a = 0.2\Delta l = \lambda_o/210$, (c) *thick*, $a = 0.48\Delta l = \lambda_o/87.5$ wires.

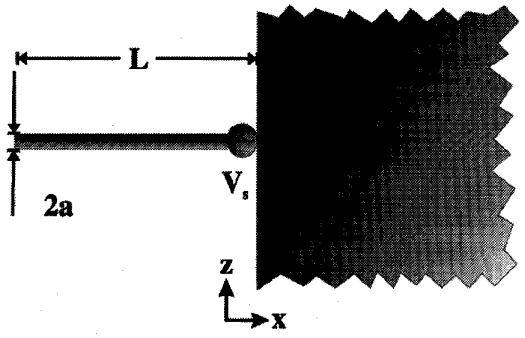

Fig. 6. A horizontal monopole attached to an infinite half-sheet.

B. Monopole Attached to a Semi-Infinite Half-Sheet

Printed circuit boards with attached cables for peripherals and power can contribute significantly to EMI. Consequently, the ability to accurately model wires extending from ground planes is important in predicting EMI from a device. An horizontal wire attached to a conducting half-sheet was also investigated with FDTD. For this case, input impedance results calculated with the method of moments are available in the literature for comparison. A voltage source was placed at the junction between the wire and the half-sheet, as shown in Fig. 6. The wire length was $\lambda_o/40$, where λ_o was the ideal quarter-wave resonance wavelength ($\lambda_o \equiv 4L$). The magnetic field components surrounding the wire and source were computed using Taflove's quasistatic approximations. The infinite half-sheet was modeled by extending the conducting plane a half-wavelength (wavelength associated with the simulated source frequency) from the source, and then truncating the plane using first- and second-order Mur absorbing boundaries. Cubic cells of dimension $\Delta l = \lambda_o/40$ were employed. Second-order Mur absorbing boundaries truncated the computational domain. The applied voltage source was swept in frequency to vary the ratio of wire length to wavelength for $0.1 \leq L/\lambda \leq 0.35$. The resulting FDTD input impedance computations were compared to the moment method results found in [12]. The bandwidth of tested frequencies was small because the published moment method data was available only up to $L/\lambda = 0.35$.

Fig. 7 shows the comparisons of the FDTD input impedance computations with moment method results for a horizontal wire with three different radii. The results of the FDTD analysis show reasonable agreement over the range of frequencies observed. In particular, the computed resistances agreed well. The resonance frequency computed with FDTD (i.e., lowest frequency for which $\mathrm{Im}\{Z_{\mathrm{input}}\} = 0$) for the *very thin* wire ($a = 0.05\Delta l$) differed from that computed by the moment method by approximately six percent. The difference in the input resistance at the resonance frequency was less than one half of one percent. The results for the *thin* wire $a = 0.1\Delta l$ resonance frequency differed by less than five percent from the moment method results. The difference between the input resistance computed at the resonance frequency with FDTD and the moment method for the thin wire was less than three percent. The *thick* wire $a = 0.2\Delta l$ results differed between the two methods by less than four percent for the resonance frequency, and five percent for the input resistance

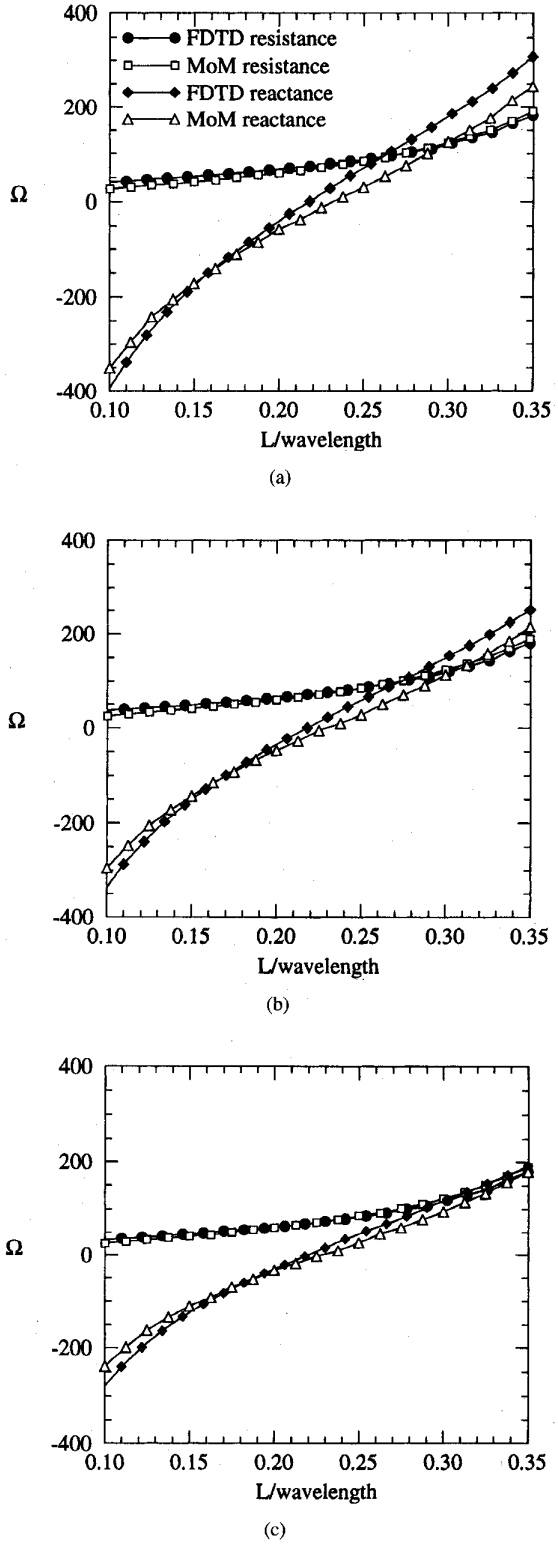

Fig. 7. Comparison of the FDTD input impedance results with moment method results for monopoles of various radii for (a) *very thin* $L/a = 200, a = 0.05\Delta l$ (b) *thin* $L/a = 100, a = 0.1\Delta l$, and (c) *thick* $L/a = 50, a = 0.2\Delta l$.

at resonance. The FDTD *thick* wire compared better with the moment method results over the entire frequency range as expected since the wire radius was approximately 20% of the unit cell length.

The monopole input impedance results show the same difficulties with modeling the steep current gradients in the source region as the full-wave resonance is approached. The errors are primarily manifested in the reactance, and are visible as L/λ approaches 0.35. The discrepencies that occur between the two computational methods may also be due in part to limitations in FDTD modeling of the semi-infinite half-sheet. The conducting sheet must contact the absorbing boundary, allowing reflections from the sheet which may be incident to the absorbing boundary at angles which are not well absorbed with second-order Mur absorbing boundary conditions.

IV. Application to EMC: Shielding Enclosure Analysis

Conducting enclosures are commonly used to contain radiation from printed circuit designs. However, the shield must be perforated with apertures and seams for cooling, input/output, and displays. In a typical enclosure design, apertures are carefully specified to avoid resonances; however, energy may couple from a resonant cavity through a nonresonant aperture to a cable located in proximity to the aperture. An improperly located cable may enhance radiation, causing the device to exceed FCC limits on emissions. Costly and time-consuming EMC retrofits are then necessary to comply with regulations. Lossy coatings may be used to lower radiation from an enclosure by supplying a significant loss mechanism. FDTD was used to model a simple enclosure and observe the emissions over a range of frequencies where a number of resonances were expected. Enclosures with external cables were considered, and internal lossy coatings were employed to lower the quality factor (Q) of the system resonances.

A. Shielding Enclosure Model

A rectangular shielding enclosure with a narrow aperture was modeled to study radiation from conducting enclosures. All dimensions reported herein were normalized to the free-space wavelength at the lowest predicted ideal (continuous rectangular cavity) TE_{101} cavity resonance,

$$\lambda_o \equiv 2\frac{1}{\sqrt{\dfrac{1}{\text{width}^2}+\dfrac{1}{\text{depth}^2}}}.$$

The computational domain was discretized with cubic cells of dimension

$$\Delta l = \frac{\lambda_o}{20} = \Delta x = \Delta y = \Delta z.$$

The differential time element was set as $\Delta t \approx (\Delta l/2c_o)$,[3] where c_o is the speed of light in free-space. The cavity model, shown in Fig. 8, had dimensions of $1.2\lambda_o \times .25\lambda_o \times 0.55\lambda_o$

[3]The differential time element was minutely changed at each frequency to allow an integer number of time steps per temporal period. An integer number of time steps is necessary for accurately computing frequency-domain quantities with the discrete Fourier transform.

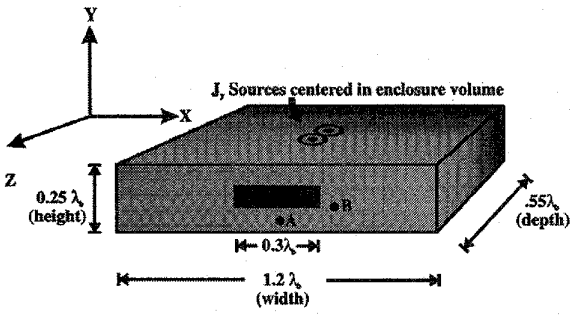

Fig. 8. Shielding enclosure with the dimensions and location of the attached cables and the aperture.

(from Node (1,1,1) to Node (25,6,12) $\Rightarrow 24 \times 5 \times 11$ cells). The enclosure walls were modeled as planar perfect electric conductors (pec's). The aperture was $0.3\lambda_o \times 0.05\lambda_o$ and centered in the pec wall horizontally and vertically [from Node (10,3,12) to Node (16,4,12)]. The cavity was excited with two 1 $\mathrm{A/cm^2}$ $\hat{y}$-polarized, current-density sources which were in phase with each other. The sources were located symmetrically in the center of the enclosure at Nodes (13,3,6–7). Second-order Mur absorbing boundaries were located one-half free-space wavelength from the enclosure. The sources were swept in frequency between $0.8 \leq f/c_o/\lambda_o \leq 1.8$. The time-averaged power through the aperture was computed at each frequency after the system reached steady-state operation. All radiated powers were normalized to the radiated power level computed for the lowest cavity resonance (TE_{101}) for the base (control) configuration of a cavity with an aperture (i.e., no attached cables or lossy coatings).

B. Shielding Enclosure with an Aperture

The sources in the control configuration (shielding enclosure with an aperture, but no attached cables or lossy coatings) were swept in frequency, and the power radiated through the aperture was determined. The power-frequency response for the control configuration is shown in Fig. 9. Approximately 25 points were computed around the peaks to ensure that a peak value had been computed. The lower resonance was the lowest cavity resonance, hereafter referenced as the TE_{101} mode resonance. This resonance was shifted down in frequency from the theoretical value for a continuous rectangular cavity because of the aperture. The aperture dimensions at the TE_{101} resonance were small relative to wavelength, resulting in large internal fields at resonance, and very little loss to the system, with a Q of over 500. For typical applications, an enclosure would have numerous apertures and seams, and Q's significantly less than 100 might be expected. The Q is defined here as the ratio of radian frequency times the average stored energy to dissipated power, which is equivalent to $f_{\mathrm{peak}}/\Delta f_{\mathrm{3dB}}$ where f_{peak} is the resonance frequency, and Δf_{3dB}, is the difference between the frequencies at which half of the peak of power is radiated [19].

The second cavity resonance, the TE_{201} mode, should have been evident at a normalized frequency of 1.233. Since the source distribution was even about the source in x, only modes with even symmetry about the source in x could be excited.

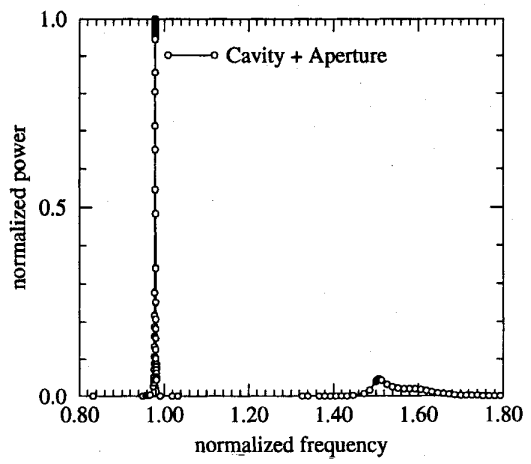

(a)

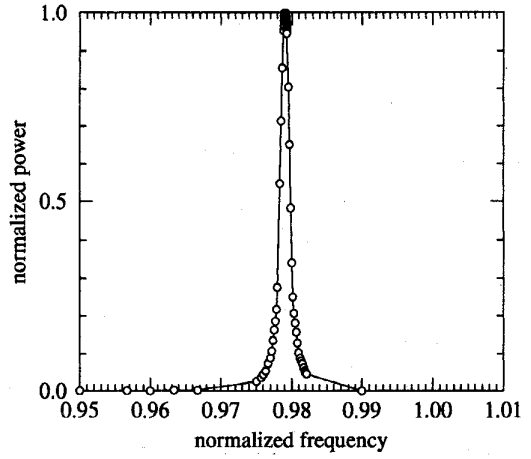

(b)

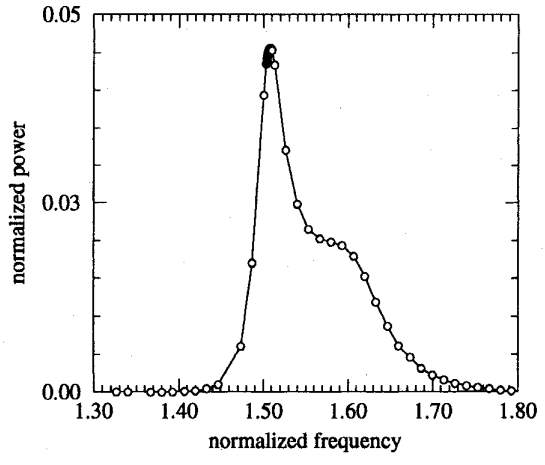

(c)

Fig. 9. Time-averaged power through the aperture as a function of frequency for the shielding enclosure with an aperture. (a) Entire frequency range, (b) enlarged view of lower resonance, and (c) enlarged view of upper resonance.

Because of the source locations, the source was orthogonal to the TE_{201} mode and did not excite it. Even modes, such as the TE_{201} mode, have a null at the center of the cavity where the sources were located, as demonstrated in Fig. 10. The resulting low energy emission demonstrated how source location can affect EMI.

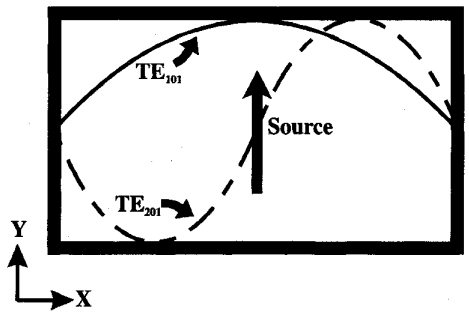

Fig. 10. An example of the modal electric field E_y distribution in the x-direction for the TE_{101} and TE_{201} modes.

The last cavity resonance within the observed frequency range (TE_{301}), expected at $f_{\text{normalized}} \approx 1.54$, was shifted down because of the loss through the aperture. The aperture had a half-wave resonance at $f_{\text{normalized}} \approx 1.67$ which was shifted down due to the finite width of the aperture. The proximity of the aperture resonance and TE_{301} mode resonance created a moderately broadband emissions region in the power-frequency response.

The magnitude of E_y at the peak resonance frequencies in the $x-z$ plane at the center of the enclosure ($j = 3$) is shown in Fig. 11. At the TE_{101} mode resonance, the aperture was small with respect to wavelength, and was therefore a poor loss mechanism, resulting in a high Q. The resulting fields in the resonant enclosure were large, and the energy that "leaked" through the aperture was considerable even though the aperture length was only slightly larger than a quarter of a wavelength. At the TE_{301} mode resonance, the aperture was larger with respect to wavelength and therefore resulted in a significant amount of loss. The peaking in the center of the field plot was a result of the current density sources. The TE_{301} field distribution was evident at the aperture half-wave resonance, as seen in Fig. 11(c), but the field strength was lower and the primary radiating mechanism was the resonant aperture.

C. Shielding Enclosure with an Aperture and Lossy Coating

A typical shielding enclosure with numerous perforations is expected to have a Q significantly less than 100. However, Q's as small as 10 can potentially cause difficulties in meeting emissions requirements for a resonance excited "ideally" in the enclosure at a low-order clock harmonic. Introducing loss into the enclosure design can decrease the Q. A lossy coating was placed over the entire wall opposite the aperture [from Node (1,1,1) to Node (25,6,2)] inside the cavity shown in Fig. 8. The coating thickness was $\lambda_o/20$ with constituitive parameters $\epsilon_r = 1.5$, and $\sigma = 2.5 \times 10^{-3}$ S/cm (commercially available resistance card values [20]). The frequency response with respect to radiated power is shown in Fig. 12. At the TE_{101} resonance, the lossy coating provided a larger loss mechanism than the small aperture, and the peak radiated power was

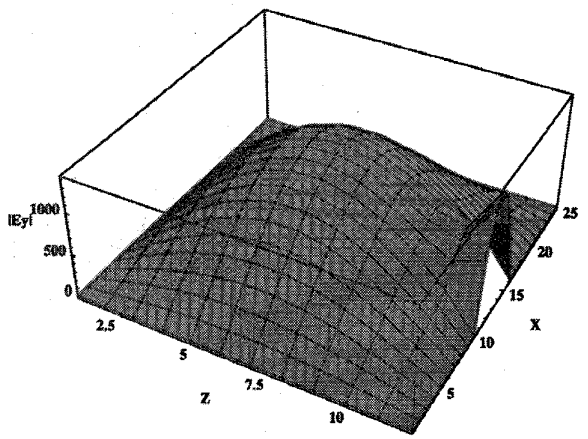

(a)

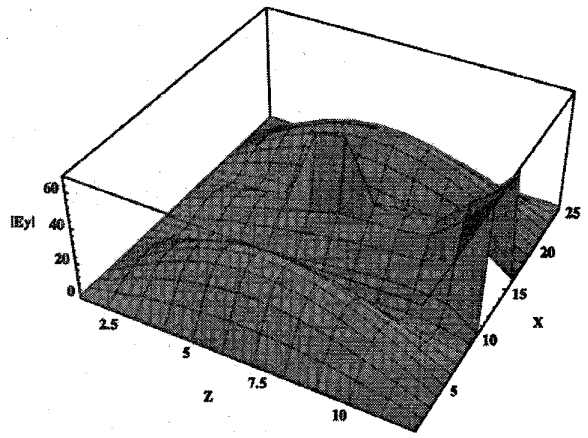

(b)

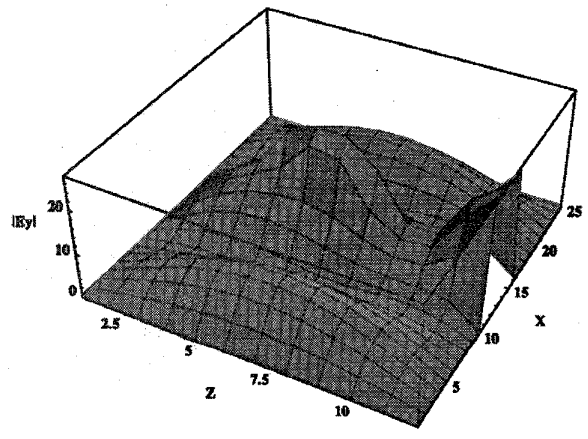

(c)

Fig. 11. Two dimensional plots showing $|E_y|$ through an $x - z$ plane where $j = 3$ for the shielding enclosure with an aperture. (a) TE_{101} mode ($f_{\text{normalized}} = 0.979$), (b) TE_{301} mode ($f_{\text{normalized}} = 1.5$), and (c) aperture half-wave resonance ($f_{\text{normalized}} = 1.6$).

reduced by almost 20 dB. The fields were reduced because the lossy coating limited the energy buildup in the resonant field distribution. At the TE_{301} mode and aperture resonance

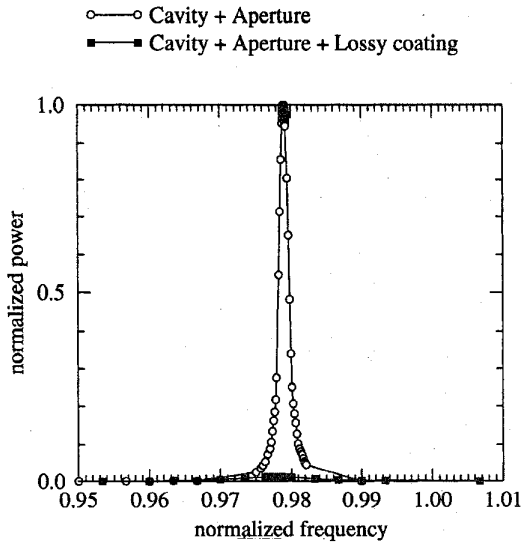

(a)

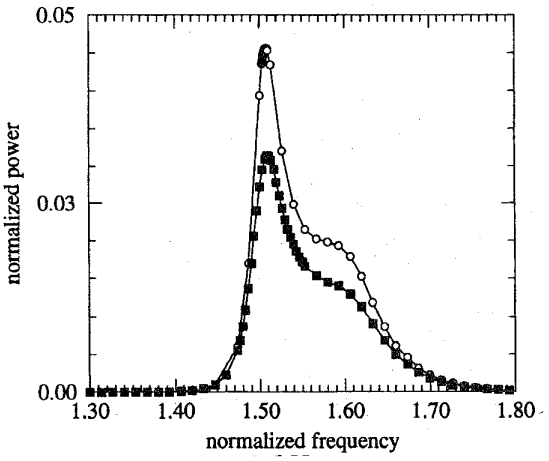

(b)

Fig. 12. Time-averaged power through the aperture as a function of frequency for the shielding enclosure with an aperture, and the shielding enclosure with an aperture and a lossy coating. (a) Enlarged view of lower resonance, and (b) enlarged view of upper resonance.

frequencies, the lossy coating was not as effective at reducing the radiated power because the aperture was electrically larger in this region, and the Q was initially much smaller than at the fundamental resonance. The loss resulting from the aperture was comparable to the loss in the coating even though the coating appeared electrically thicker at the higher frequencies.

D. Shielding Enclosure with an Aperture and Attached Wire

Energy coupling between apertures and attached cables was also investigated. The radiated power was computed for the enclosure with a wire attached to the shield face containing the aperture. The time-averaged power through the aperture as a function of frequency is shown in Fig. 13 for a wire attached at location A, and then at location B (see Fig. 8). A shielded cable was modeled with Taflove's quasistatic field approximation as described in Section II. The wire connection

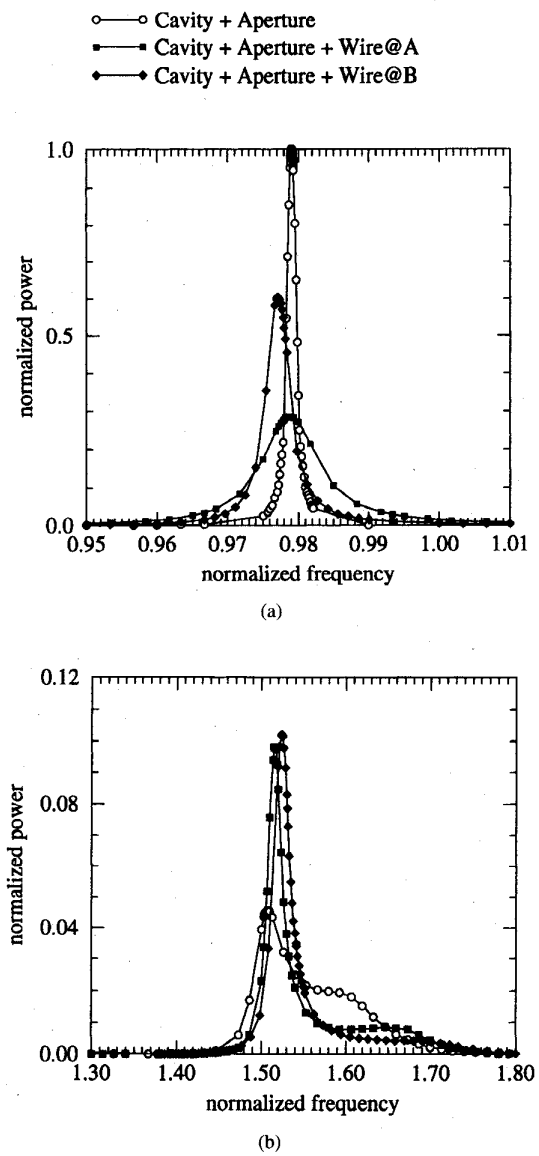

Fig. 13. Time-averaged power through the aperture as a function of frequency for the shielding enclosure with an aperture, the shielding enclosure with an aperture and a wire attached at A, and the shielding enclosure with an aperture and a wire attached at B. (a) Enlarged view of lower resonance, and (b) enlarged view of upper resonance.

to the shield was modeled by using quasistatic approximations to compute the magnetic field components surrounding the wire, and setting the electric field components along the wire axis and tangential to the enclosure shield to zero. This configuration was employed to model a shielded cable attached to the enclosure with a 360° connection. The wire had a length of $\lambda_o/5$ $(4\Delta l)$ and a radius of $\lambda_o/250$. The wire was located alternately at points A and B in Fig. 8, where point A was horizontally centered and $\lambda_o/20$ below the edge of the aperture at Node (13,2,12), and B was $\lambda_o/20$ to the right of the lower right-hand corner of the aperture at Node (17,4,12). The wire should have had a quarter-wave resonance frequency of $f_{\text{normalized}} \approx 1.25$. As previously discussed, the field structure in the cavity at this frequency had an odd distribution in x about the source, which was prohibited by the placement of the source in the center of the cavity.

The attached shielded cable reduced the power radiated through the aperture at the TE_{101} resonance. Equivalence theory can be employed to replace the electric field over the aperture in a pec plane with magnetic current sources for discussion purposes. At lower frequencies, the aperture was short with respect to wavelength and the magnetic currents looked like a short magnetic dipole. The wire attached at A was located where the $\hat{z}$-component of the electric field was at a maximum in the magnetic dipole field distribution. Energy coupled efficiently to the wire at A, providing an effective loss mechanism. The Q at the TE_{101} resonance was consequently reduced. The wire at B was located where the $\hat{z}$-component of the electric field for an equivalent magnetic dipole was small; therefore the Q was not reduced to the same degree as with the wire located at A.

At the TE_{301} mode resonance frequency, the addition of the wires "tuned" the system resulting in an increased Q. The peak radiated power was increased by approximately 4 dB. In addition, the wire can potentially increase the directivity of the radiated energy. The FCC guidelines limit maximum field strength, and therefore the addition of shielded cables to the system may make the device fail emissions testing as a result of both tuning a resonance and directing energy. Further study is necessary to understand the mutual coupling between the aperture and shielding cables, as well as potential energy directivity by the wire.

V. Conclusion

Cables attached to printed circuit boards and shielding enclosures often comprise one-half of an EMI "antenna," which can result in common-mode radiation from printed circuit and enclosure designs. The resonance frequencies of the EMI antennas are a function of cable radius as well as length. Therefore, wires and cables must be modeled carefully if accurate results are to be obtained from numerical modeling techniques such as FDTD. The simplest FDTD wire-modeling method sets the axial component of the electric field to zero; however, the wire radius is then a function of the grid discretization which may yield inaccurate results. Another simple option may be to use a finer mesh and model the wire with a complete FDTD cell, but this can require considerable additional memory even when employing multigrid techniques. Taflove's subcellular thin-wire modeling algorithm was found to be a computationally efficient alternative. This algorithm was used to model a dipole antenna and monopole extended from a half-plane. Odd-integer half-wave resonance frequencies and input impedance were predicted with an accuracy adequate for most EMC applications. Integer wavelength resonance frequencies and input impedance were not predicted well with the quasistatic approximation for very-thin wires $(a \approx 0.0005\lambda_o)$, however, for thicker wires or cables $(a \approx 0.01\lambda_o)$, the accuracy may be acceptable in many cases.

A shielding enclosure was modeled to demonstrate the utility of the FDTD method in EMC applications and the quasistatic approximation for thin wires in simulating common-

mode radiation from enclosures and printed circuit designs with attached cables. High Q systems were found to yield higher radiation when a system resonance was excited, indicating that loss mechanisms are important in reducing EMI. A lossy dielectric coating was used to demonstrate the effect of a judicious use of loss. Wires attached to the enclosure were modeled using Taflove's quasistatic thin-wire algorithm. The model demonstrated how energy coupled to attached wires through an aperture can increase the Q of the system near one of the cavity resonances, causing radiated emissions to increase. The quasistatic thin-wire algorithm was found to be an efficient method for modeling wires by which the coupling mechanisms leading to common-mode radiation involving wires may be further studied.

REFERENCES

[1] K. S. Kunz and R. J. Luebbers, *The Finite Difference Time Domain Method for Electromagnetics*. Boca Raton, FL: CRC Press, 1993.

[2] A. Taflove, *Computational Electrodynamics: The Finite-Difference Time-Domain Method*. Boston, MA: Artech House, 1995.

[3] J. L. Drewniak, T. H. Hubing, and T. P. Van Doren, "Investigation of fundamential mechanisms of common-mode radiation from printed circuit boards with attached cables," in *1994 IEEE Int. Symp. Electromag. Compat.*, IEEE Electromag. Compat. Soc., Aug. 1994, pp. 110–115.

[4] T. Hubing and J. F. Kaufman, "Modeling the electromagnetic radiation from electrically small table-top products," *IEEE Trans. Electromag. Compat.*, vol. 31, pp. 74–84, Feb. 1989.

[5] J. L. Drewniak, Fei Sha, T. H. Hubing, T. P. Van Doren, and J. Shaw, "Diagnosing and modeling common-mode radiation from printed circuit boards with attached cables," in *1995 IEEE Int. Symp. Electromag. Compat.*, IEEE Electromag. Compat. Soc., Aug. 1995.

[6] J. G. Maloney, G. S. Smith, and Jr. W. R. Scott, "Accurate computation of the radiation from simple antennas using the finite-difference time-domain method," *IEEE Trans. Antennas Propagat.*, vol. 38, pp. 1059–1068, July 1990.

[7] R. Holland and L. Simpson, "Finite-difference analysis of EMP couping to thin struts and wires," *IEEE Trans. Electromag. Compat.*, vol. 23, pp. 88–97, May 1981.

[8] K. R. Umashankar, A. Taflove, and B. Beker, "Calculation and experimental validation of induced currents on coupled wires in an arbitrary shaped cavity," *IEEE Trans. Antennas Propagat.*, vol. 35, pp. 1248–1257, Nov. 1987.

[9] A. Taflove, K. Umashankar, B. Beker, F. Harfoush, and K. Yee, "Detailed FD-TD analysis of electromagnetic fields penetrating narrow slots and lapped joints in thick conducting screens," *IEEE Trans. Antennas Propagat.*, vol. 36, pp. 247–257, Feb. 1988.

[10] R. Luebbers, L. Chen, T. Uno, and S. Adachi, "FDTD calculation of radiation patterns, impedance, and gain for a monopole antenna on a conducting box," *IEEE Trans. Antennas Propagat.*, vol. 40, pp. 1577–1583, Dec. 1992.

[11] G. J. Burke and A. J. Poggio, *Numerical Electromagnetics Code (NEC)—Method of Moments*. Livermore National Laboratory, UCID-18834, 1981.

[12] K. Sawaya, T. Ishizone, and Y. Mushiake, "A simplified expression of the dyadic Green's function for a conducting half-sheet," *IEEE Trans. Antennas Propagat.*, vol. 29, pp. 749–756, Sept. 1981.

[13] T. Wang, A. Cuevas, and H. Ling, "RCS of a partially open rectangular box in the resonant region," *IEEE Trans. Antennas Propagat.*, vol. 38, pp. 1498–1504, Sept. 1990.

[14] T. Wang and H. Ling, "Electromagnetic scattering from three-dimensional cavities via a connection scheme," *IEEE Trans. Antennas Propagat.*, vol. 39, pp. 1505–1513, Oct. 1991.

[15] A. Taflove and K. Umashankar, "The finite-difference time-domain method for numerical modeling of electromagnetic wave interactions," *Electromag.*, vol. 10, pp. 105–126, 1990.

[16] W. Stutzman and G. Thiele, *Antenna Theory and Design*. New York: Wiley, 1981.

[17] J. P. Berenger, "A perfectly matched layer for the absorption of electromagnetic waves," *J. Computat. Phys.*, vol. 114, no. 2, pp. 185–200, 1994.

[18] C. A. Balanis, *Antenna Theory: Analysis and Design*. New York: Wiley, 1982.

[19] D. M. Pozar, *Microwave Engineering*. Reading, MA: Addison-Wesley, 1990.

[20] C. W. Penney and R. J. Luebbers, "Input impedance, radiation pattern, and radar cross section of spiral antennas using FDTD," *IEEE Trans. Antennas Propagat.*, vol. 42, pp. 1328–1332, Sept. 1994.

David M. Hockanson (S'90) received the B.S. and M.S. degrees in electrical engineering from the University of Missouri-Rolla in 1992 and 1994, respectively.

His research and education endeavors have been supported by scholarships, fellowships, and assistantships at Rolla, the most recent being a National Science Foundation Graduate Fellowship. His research interests include numerical and experimental analysis of electromagnetic compatibility problems. Previous work has involved digital power bus design and shielding enclosure design. Presently, he is working on experimental investigations and equivalent circuit development of noise sources and radiation mechanisms on printed circuit board geometries.

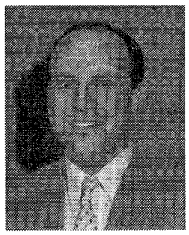

James L. Drewniak (S'85–M'90) received the B.S. (highest honors), M.S., and Ph.D. degrees in electrical engineering from the University of Illinois at Urbana-Champaign in 1985, 1987, and 1991, respectively.

He was the recipient of several graduate fellowships and awards at the University of Illinois, and pursued his graduate studies in wave propagation and interactions in the areas of electromagnetics, antennas, microwaves, and acoustics. In July 1991, he joined the Electrical Engineering Department at the University of Missouri-Rolla as an Assistant Professor and has received campus Teaching Excellence Awards for 1991 and 1992. His research interests include the development and application of numerical methods for investigating electromagnetic compatibility problems, antenna analysis, and modeling of microwave components, as well as experimental studies in antenna and electromagnetic compatibility problems.

Dr. Drewniak is Secretary/Treasurer of the Rolla IEEE Subsection, an Associate Editor for the Applied Computational Electromagnetics Society newsletter, and is also a member of the Acoustical Society of America, Eta Kapa Nu, Tau Beta Pi, Sigma Xi, and Phi Kappa Phi.

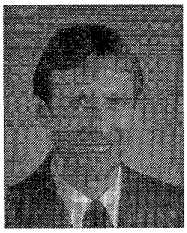

Todd H. Hubing (S'82–M'82–SM'93) received the B.S.E.E. degree from the Massachusetts Institute of Technology in 1980, the M.S.E.E. degree from Purdue University in 1982, and the Ph.D. degree in electrical engineering from North Carolina State University in 1988.

From 1982 to 1989, he was employed in the Electromagnetic Compatibility Laboratory at IBM Communications Products Division in Research Triangle Park, NC. He is currently an Associate Professor in Electrical Engineering at the Unviersity of Missouri-Rolla. Since joining UMR in 1989, he has earned an Outstanding Teaching award and two awards for faculty excellence. His primary area of research involves the development and application of numerical methods for solving problems in electromagnetic compatibility.

Dr. Hubing is the Treasurer of the Applied Computational Electromagnetics Society and he is the Director of Member Services for the IEEE EMC Society. He also writes the "Chapter Chatter" column for the IEEE EMC Society Newsletter.

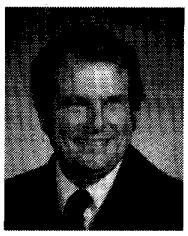

Thomas P. Van Doren (M'58) received the B.S., M.S., and Ph.D. degrees from the University of Missouri-Rolla in 1962, 1963, and 1969, respectively.

From 1963 to 1965, he served as an Officer in the U.S. Army Security Agency. From 1965 to 1967, he was a Microwave Engineer with Collins Radio Company. Since 1967, he has been a member of the electrical engineering faculty at the University of Missouri-Rolla, where he is currently a Professor. His research interests concern developing circuit layout, grounding, and shielding techniques to improve electromagnetic compatibility. He has taught short courses on electromagnetic compatibility to over 10,000 engineers and technicians representing 200 corporations.

Dr. Van Doren received an IEEE EMC Society Richard R. Stoddard Award for his contributions to EMC research and education in 1995. He is a Registered Professional Engineer in the state of Missouri and a member of Eta Kappa Nu, Tau Beta Pi, and Phi Kappa Phi.